Supplementary Materials

Two-Step Dry Gel Method Produces MgAPO-11 with Low Aspect Ratio and Improved Catalytic Performance in the Conversion of Methanol to Hydrocarbons

Lina Zhang [1,2], Daniel Sean Firth [1], Unni Olsbye [1,*] and Xiaojun Bao [3]

[1] Center for Materials Science and Nanotechnology, Department of Chemistry, University of Oslo, P.O. Box 1033 Blindern, N-0315 Oslo, Norway; upczhlina@163.com (L.Z.); danielfirth.mail@gmail.com (D.S.F.)
[2] Sinopec Beijing Research Institute of Chemical Industry, Beijing 100728, China
[3] National Engineering Research Center of Chemical Fertilizer, College of Chemical Engineering, Fuzhou University, Fuzhou 350116, China; baoxj@fzu.edu.cn
* Correspondence: unni.olsbye@kjemi.uio.no; Tel.: +47-22-85-54-56

Abstract: In this article, the synthesis, characterization and catalytic performance of three MgAPO-11 catalysts with distinct crystal morphologies (sunflower, ball and candy) are presented. Among the three samples, the candy-like MgAPO-11-C, with high crystallinity and uniform particle size (of about 1 μm), was synthesized for the first time by using a unique two-step dry gel method. Despite the similar acid strength of the three samples, the different and distinct morphologies of the catalysts resulted in very different methanol-to-hydrocarbons (MTH) performances. In particular, the candy-like MgAPO-11-C presented the best MTH performance with the highest total conversion capacity (4.4 $g_{MeOH} \cdot g_{catalyst}^{-1}\ h^{-1}$) and the best selectivity to C_{5+} aliphatics (64%).

Keywords: MgAPO-11; methanol to hydrocarbons; dry gel method; crystal morphology; candy like

Table S1. Amount and distribution of acid sites of MgAPO-11 with different Mg contents.

Amount (μmol/g) and distribution of acid sites						
Sample	**Total acid sites (200 °C)**			**Strong acid sites (350 °C)**		
	B	**L**	**B+L**	**B**	**L**	**B+L**
MgAPO-11-C-0Mg	4	26	30	4	9	13
MgAPO-11-C-0.1Mg	31	76	107	9	67	76
MgAPO-11-C-0.2Mg	14	60	74	4	29	33

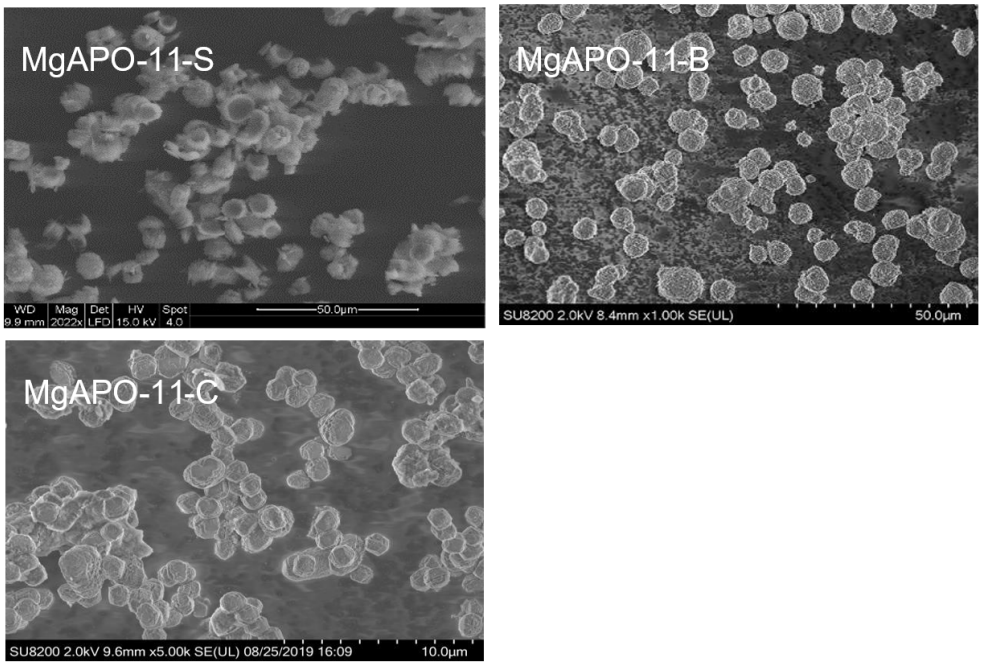

Figure S1. SEM images of the three MgAPO-11 samples with distinct morphologies in low magnification.

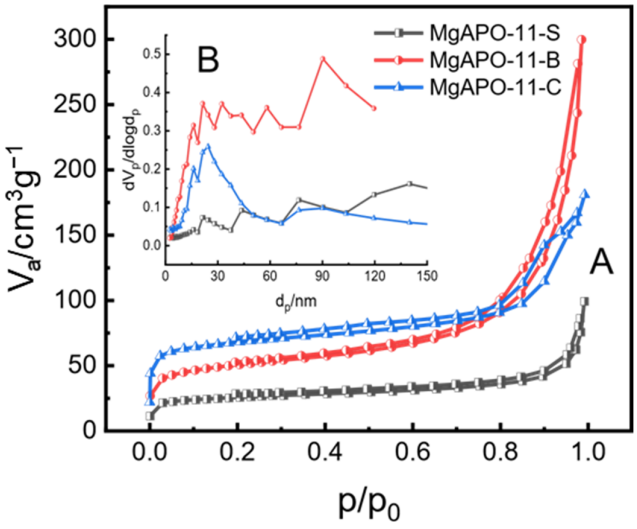

Figure S2. N_2 adsorption-desorption isotherms (**A**) and pore-size distribution patterns of the three MgAPO-11 samples with distinct morphologies (**B**).

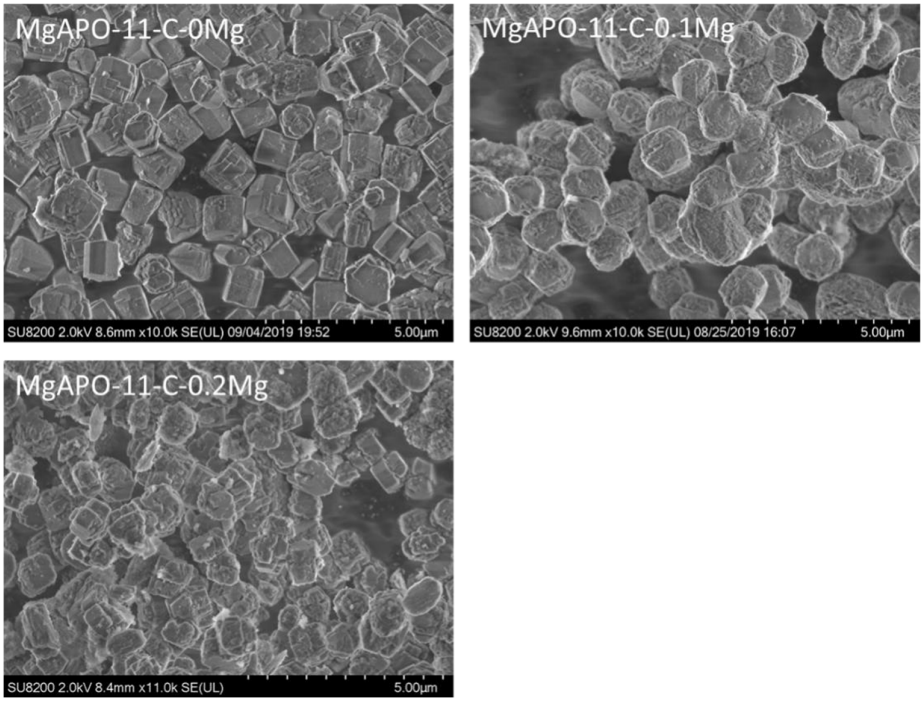

Figure S3. SEM images of MgAPO-11-C samples with different Mg contents.

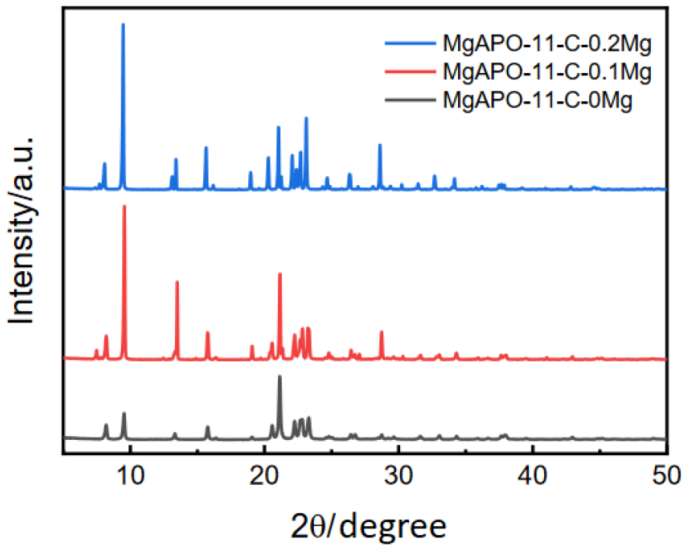

Figure S4. XRD patterns of the MgAPO-11-C samples with different Mg contents.

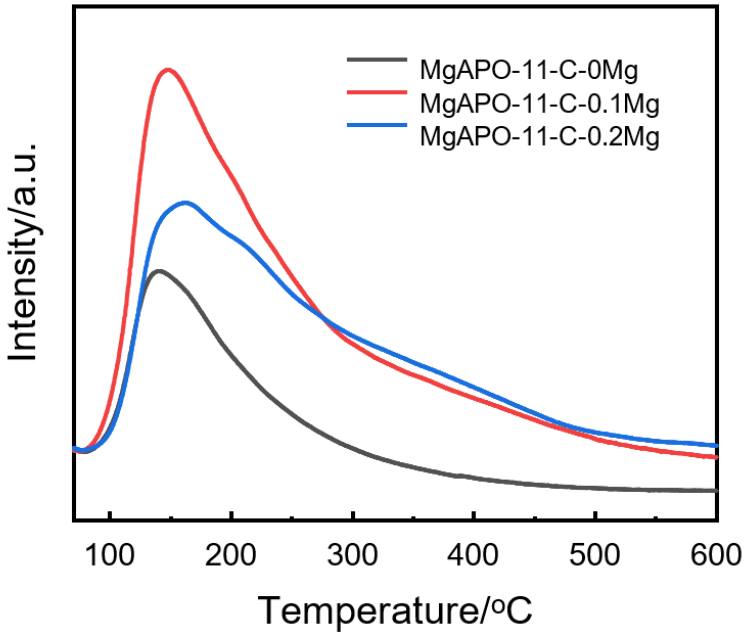

Figure S5. NH_3-TPD profiles of the MgAPO-11-C samples with different Mg contents.

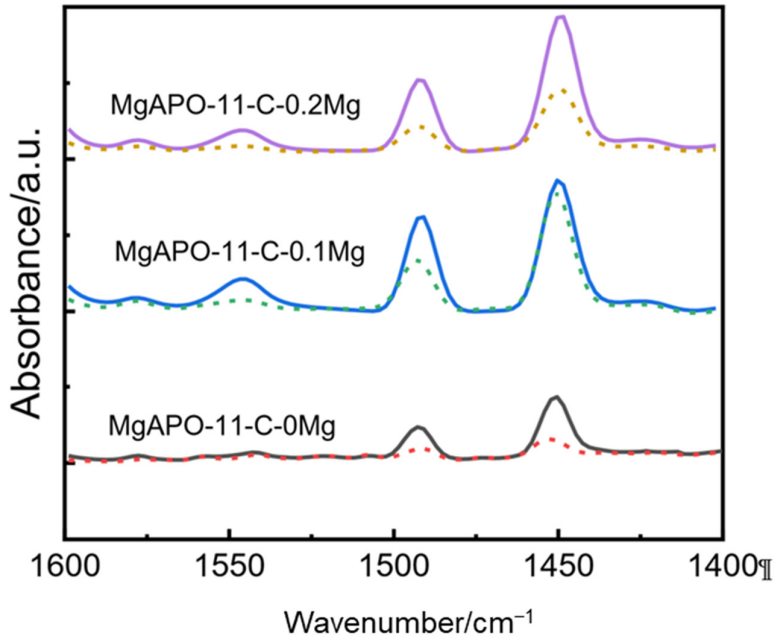

Figure S6. Py-IR spectra of MgAPO-11 with different Mg contents.

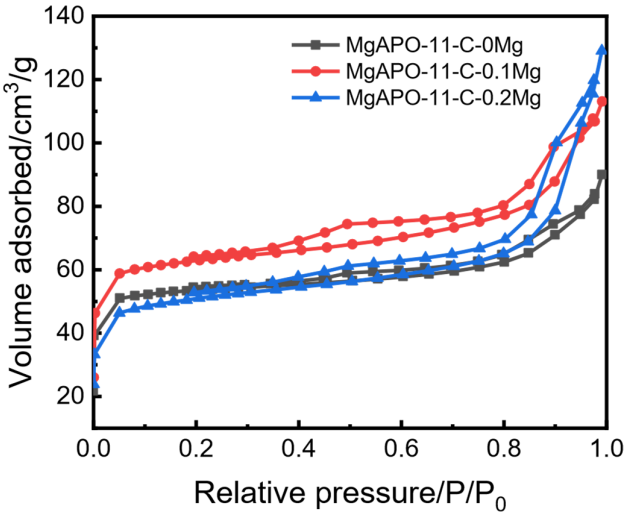

Figure S7. N_2 adsorption and desorption isotherms of the MgAPO-11-C samples with different Mg contents.

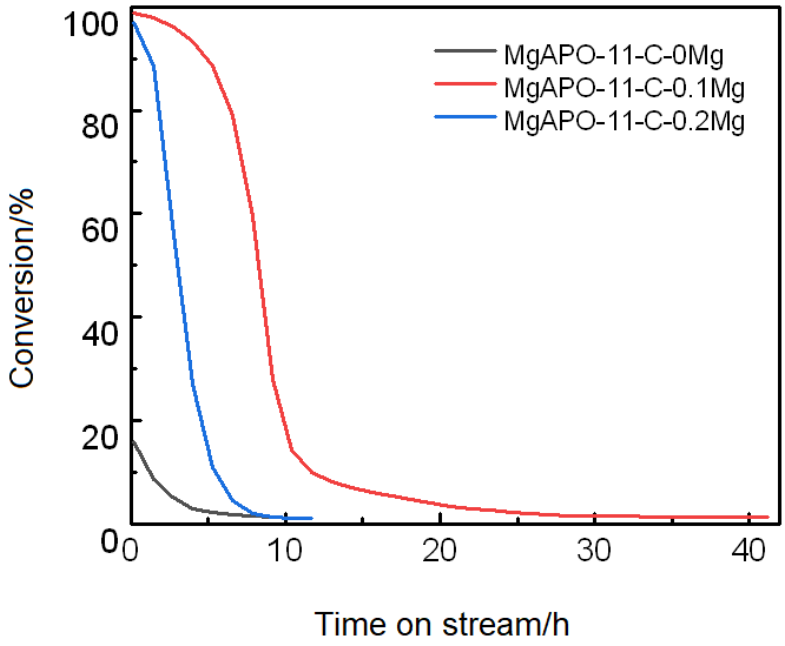

Figure S8. Methanol conversion as a function of time on stream of the MgAPO-11-C samples with different Mg contents.

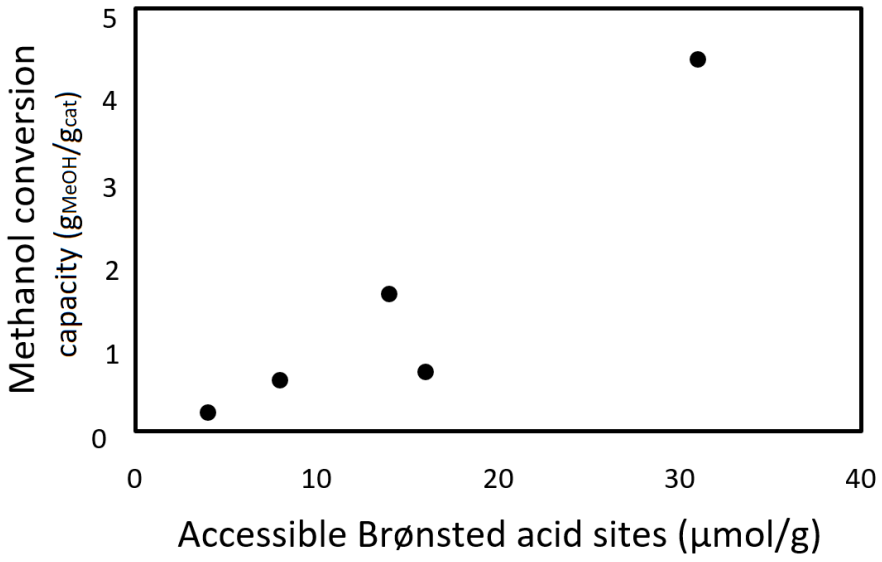

Figure S9. Methanol conversion capacity vs. accessible Brønsted acid sites in the five MgAPO-11 samples.

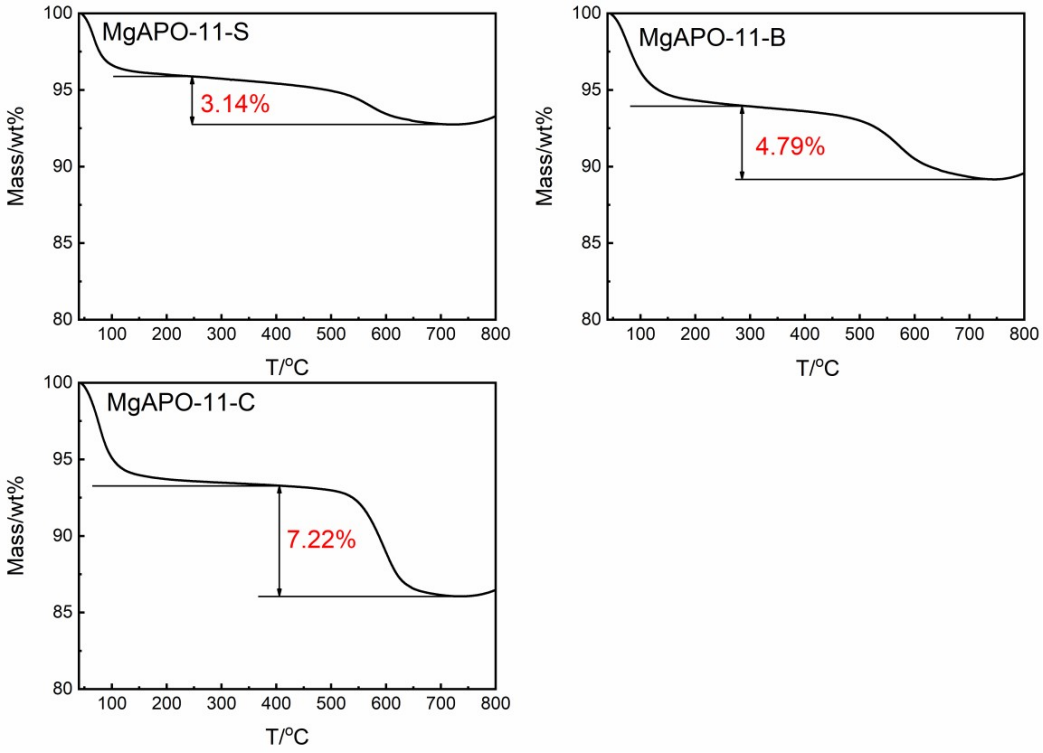

Figure S10. The TG curves of the three MgAPO-11 samples with distinct morphologies after reaction.

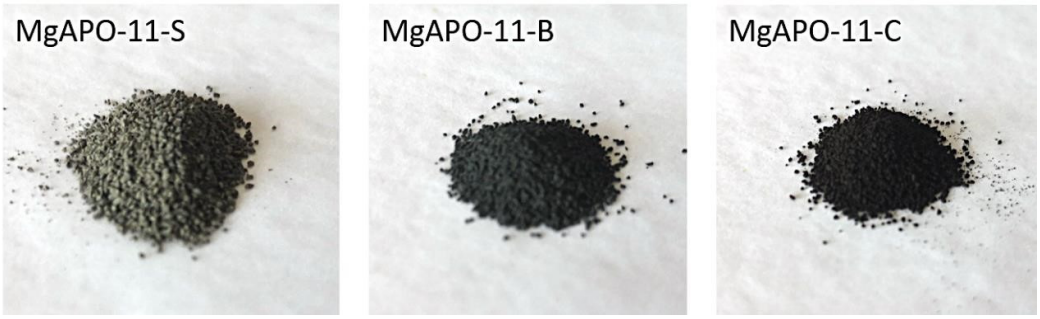

Figure S11. The photos of the three MgAPO-11 samples after reaction.